Scavenging of acidic gases (HCOOH, CH 3 COOH, HNO 3 , HCl, and SO 2) and ammonia in mixed liquid-solid water clouds at the Puy de Dôme mountain (France)

Didier Voisin, Michel Legrand, Nadine Chaumerliac

JOURNAL OF GEOPHYSICAL RESEARCH, VOL. 105, NO. D5, PAGES 6817-6835, MARCH 16, 2000

Scavenging of acidic gases (HCOOH, CH_3COOH, HNO_3, HCl, and SO_2) and ammonia in mixed liquid-solid water clouds at the Puy de Dôme mountain (France)

Didier Voisin and Michel Legrand
Laboratoire de Glaciologie et Géophysique de l'Environnement, CNRS
Saint Martin d'Hères, France

Nadine Chaumerliac
Laboratoire de Météorologie Physique, Observatoire de Physique du Globe de Clermont-Ferrand
Université Blaise Pascal, CNRS, Aubière, France

Abstract. In order to study scavenging processes of chemical species in mixed phase clouds, in-cloud field measurements were conducted in December 1997 at the Puy de Dôme mountain (center of France, 1465 m above sea level). Soluble species including NH_4^+, Cl^-, NO_3^-, SO_4^{--}, $HCOO^-$, CH_3COO^-, and $C_2O_4^{--}$ present in the different phases (supercooled water droplets, rimed snowflakes, interstitial gases, and aerosols) of cold clouds have been investigated. Conducted in parallel to microphysical studies of clouds (liquid water and ice contents, and size distribution of hydrometeors), these chemical investigations allow us to examine the partitioning of strong (HNO_3 and HCl) and weak (SO_2, HCOOH, and CH_3COOH) acids as well as ammonia between interstitial air and the condensed phases (liquid and solid water particles) in mixed clouds present during winter at midlatitude regions. From that, we discuss the processes by which these key atmospheric species are taken up from the gas phase by the condensed phases (liquid and ice) in these cold clouds. We examine several factors which are of importance in driving the final composition of cloud ice. They include the partitioning of species between gaseous and supercooled liquid phases, the amount of rimed ice collected by snowflakes, and the retention of gas during shock freezing of supercooled droplets onto ice particles. Strong acids (HCl and HNO_3) as well as NH_3, being sufficiently soluble in water, are mainly partitioned into supercooled water droplets. Furthermore, being subsaturated in liquid droplets, these species are well retained in rimed ice. For these species, riming is found to be the main process driving the final composition of snowflakes, direct incorporation from the gas phase during growth of snowflakes remaining insignificant because of low concentrations in the gas phase. For light carboxylic acids the riming process mainly determines the composition of the snowflakes, but an additional significant contribution by gas incorporation during the growth of snowflakes cannot be excluded. SO_2 is also present at significant levels in the interstitial air and is poorly retained in ice during riming of supercooled water droplets. However, hydroxymethanesulfonate (HMSA) was likely present in supercooled liquid droplets, making it difficult to evaluate by which mechanism S(IV) (i.e., HMSA plus SO_2) has been incorporated into snowflakes.

1. Introduction

Chemical species of interest for the tropospheric chemistry, either directly emitted from surface sources or produced within the atmosphere, are eliminated from the atmosphere through photolysis, homogeneous (gas phase) and/or heterogeneous chemistry, and dry and wet deposition processes. Chemical processes converting emitted gases into secondary chemical species can proceed on aerosols as well as in the aqueous phase of clouds. Clouds therefore represent active systems controlling in a large extent steady state concentrations of various key components of the troposphere. Because of this importance of clouds in the tropospheric chemistry, numerous studies have been dedicated to the cloud chemistry. Previous studies have been dedicated to the partitioning of several atmospheric gases including carboxylic acids [*Winiwarter et al.*, 1988; *Facchini et al.*, 1992; *Sanhueza et al.*, 1992; *Keene et al.*, 1995], NH_3, SO_2, and HNO_3 [*Winiwarter et al., 1994*; *Laj et al.*, 1997; *Ricci et al.*, 1998] between air and liquid droplets present in clouds or fogs. Large deviations of several orders of magnitude with the

Paper number 1999JD900983.
0148-0227/00/1999JD900983$09.00

theoretical Henry's law equilibrium were found in most cases, showing either sub-saturation or super-saturation of species in the liquid phase. Several processes may contribute to these observed departures from the equilibrium including mixing of droplets at different pH [*Pandis and Seinfeld*, 1991], variations of the liquid water content during sampling [*Winiwarter et al.*, 1992], mass transfer limitation of highly soluble species [*Winiwarter et al.*, 1994; *Ricci et al.*, 1998], and possibly liquid phase chemical reactions.

Since water readily supercools, cold clouds frequently contain liquid droplets between 0° and -10°C. At temperatures close to -10°C the presence of ice particles becomes frequent (50% of cases at -10°C [*Pruppacher and Klett*, 1997]). Clouds present at midlatitudes being frequently mixed (supercooled liquid and ice) systems, there is therefore a strong need to evaluate the role of the ice with respect to the liquid phase in scavenging numerous gaseous species. In cold clouds the ice grows at the expense of the liquid water phase. This occurs either by collision of liquid droplets with ice particles followed by shock freezing (riming process) for large enough ice crystals or by diffusion of water vapor to the ice because of the lower vapor pressure of ice with respect to water (Wegener-Bergeron-Findeisen mechanism [*Pruppacher and Klett*, 1997]). *Borys et al.* [1988] demonstrated that nucleation of cloud droplets followed by ice crystal riming is the main process in taking up aerosols in mixed clouds, the collision of ice particles with interstitial aerosols remaining an inefficient process (Figure 1). During the freezing of supercooled liquid droplets, solutes present as salts will be segregated by the ice leading to an inhomogeneous distribution in the formed ice particle, but the bulk chemistry of rimed droplets will not differ from that of supercooled droplets. The incorporation of gaseous species into ice particles of mixed clouds can occur by solubilization of gases in supercooled liquid droplets followed by ice crystal riming, by cocondensation of gaseous species along with water molecules during the growing process, and by adsorption onto the ice surface (Figure 1). In contrast to solutes built up from the solubilization of aerosols, the segregation by the ice formed during the riming process can here lead to a loss toward the gas phase, hence modifying the initial bulk composition of supercooled water droplets. Thus, for gas species, four topics need to be addressed in evaluating the role of ice in mixed clouds: as for liquid clouds, the partitioning between gas and supercooled liquid droplets with respect to the Henry's law equilibrium, and specific to mixed clouds, the rime mass fraction of ice particles, the retention coefficient of gases during riming, and the incorporation of gases during the growth of the crystal by water vapor diffusion. The poor knowledge we have of those parameters precludes any attempt to provide a realistic approach of the role of mixed clouds in the tropospheric chemistry.

The study of these incorporation mechanisms requires investigations of the microphysical characteristics of clouds as well as of the chemical composition of each phase of cloud systems. Field experiments were conducted with this aim at the Puy de Dôme mountain in December 1997 when cold clouds enveloped the site. Interstitial gases and aerosols, supercooled liquid droplets impacted in a fog collector, were sampled, as well as snow crystals when present. Ion chromatography (IC) measurements were performed on the samples collected in the different phases of clouds and include

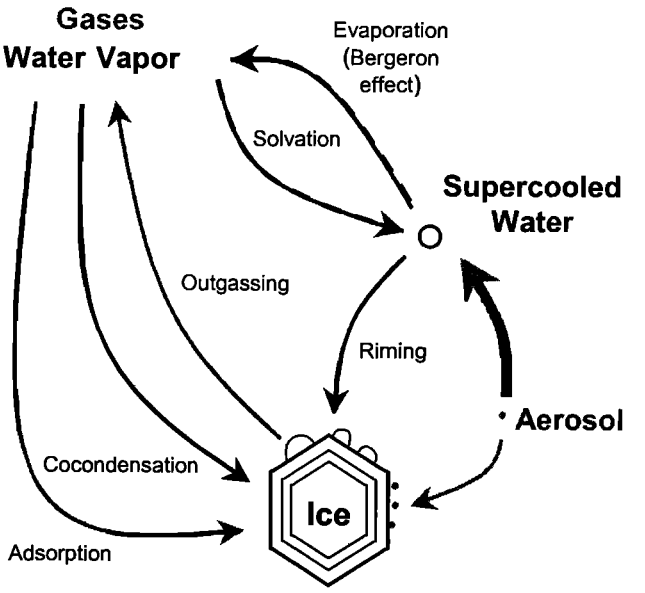

Figure 1. Schematic display of microphysical processes responsible for incorporation of aerosols and gases into supercooled liquid and ice phases of mixed clouds.

NH_4^+, Cl^-, NO_3^-, SO_4^{--}, $HCOO^-$, CH_3COO^-, and $C_2O_4^{--}$. Microphysical measurements include liquid water content, size distribution of water droplets, and size and shape of ice crystals. These data allow us to investigate the partitioning between condensed phases (supercooled liquid droplets and ice particles) and the gas phase for HCl, HNO_3, SO_2, HCOOH, and CH_3COOH. We also attempt to evaluate the respective contribution of riming and gas diffusion during the growth of the ice in controlling the final composition of snowflakes.

2. Site, Weather Conditions, and Sampled Clouds Events

In-cloud samplings took place at the Puy de Dôme mountain (45°75'N, 3°E, 1465 m above sea level) in the center of France during two periods: from December 2 to 5 (event 1) and from December 12 to 13 (event 2). Cloud event 1 was generated when a cool polar air mass located behind an active cold front reached the site at 0600 UT, December 2, 1997. Temperature, barometric pressure, and wind velocity are reported for this event in Figure 2a. From slightly positive values during the night, the temperature rapidly dropped to -8°C at 1000 UT, December 2. From December 2 to 6, temperatures fluctuated between -5° and -9°C. Over this time period, clouds continuously shrouded the site, and significant snowfalls occurred, particularly on December 3 and 4. Cloud event 2 also took place in a cool air mass (temperatures ranged from -1° to -4°C, Figure 2b) with a stalled cold front becoming an occluded front. Intermittent snow fell on December 12 in the afternoon and evening and then stopped on December 13. There were occasional breaks in the cloud during samplings at the end of event 2. During these two events, we sampled interstitial air (water soluble gases and aerosols), supercooled liquid water, and snow precipitation when occurring. Timing of these samplings is summarized in Figure 3.

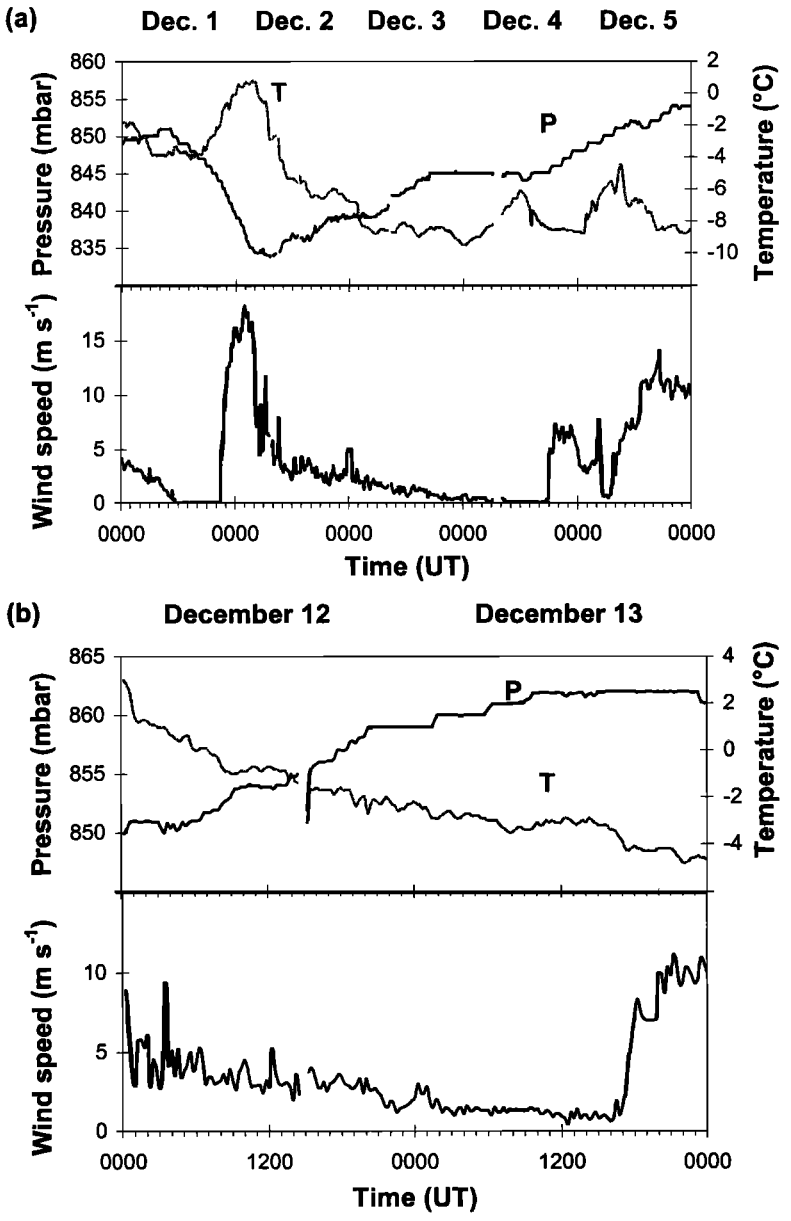

Figure 2. Temperatures, barometric pressures, and wind velocities during (a) event 1 (December 2-5, 1997) and (b) event 2 (December 12-13, 1997). During both events, relative humidity remained 100%.

3. Sampling and Methods

3.1. Cloud Microphysics

During the two cloud events, the liquid water content (LWC) was monitored by a particulate volume monitor (PVM 100), a laser diffraction particle-sizing instrument [*Gerber*, 1991]. This probe also provides the effective radius of liquid water droplets in the range of 2-32 μm. On December 3, PVM data are not available, and we hence used data provided by the axially scattering spectrometer probe (ASSP), which sizes water droplets with diameter ranging from 2 to 47 mm [*Dye and Baumgardner*, 1984]. When ice particles are present, their size distributions (50-2000 μm) were monitored with a two-dimensional optical array probe (OAP 2D), which analyzes the cast shadow of individual ice particles [*Knollenberg*, 1970]. This probe was operating on December 3 in the afternoon and on December 4, providing ice content (ICC), and concentration and diameter (largest dimension) of ice particles (Figure 4).

3.2. Gas and Aerosol Sampling

Reliable in-cloud interstitial air (gas as well as aerosol) sampling cannot be achieved without eliminating the cloud droplets from the sample stream. We here used an inertial droplet separator that prevents contact between cloud droplets and interstitial gases. The general design and efficiency of our system (Figure 5a) are similar to that of the separator previously developed by *Munger et al.* [1995]. The cutoff diameter is estimated to be close to 1 μm, thus being sufficient to prevent gas sampling from water droplet interference.

To evaluate the collection efficiency of our device in

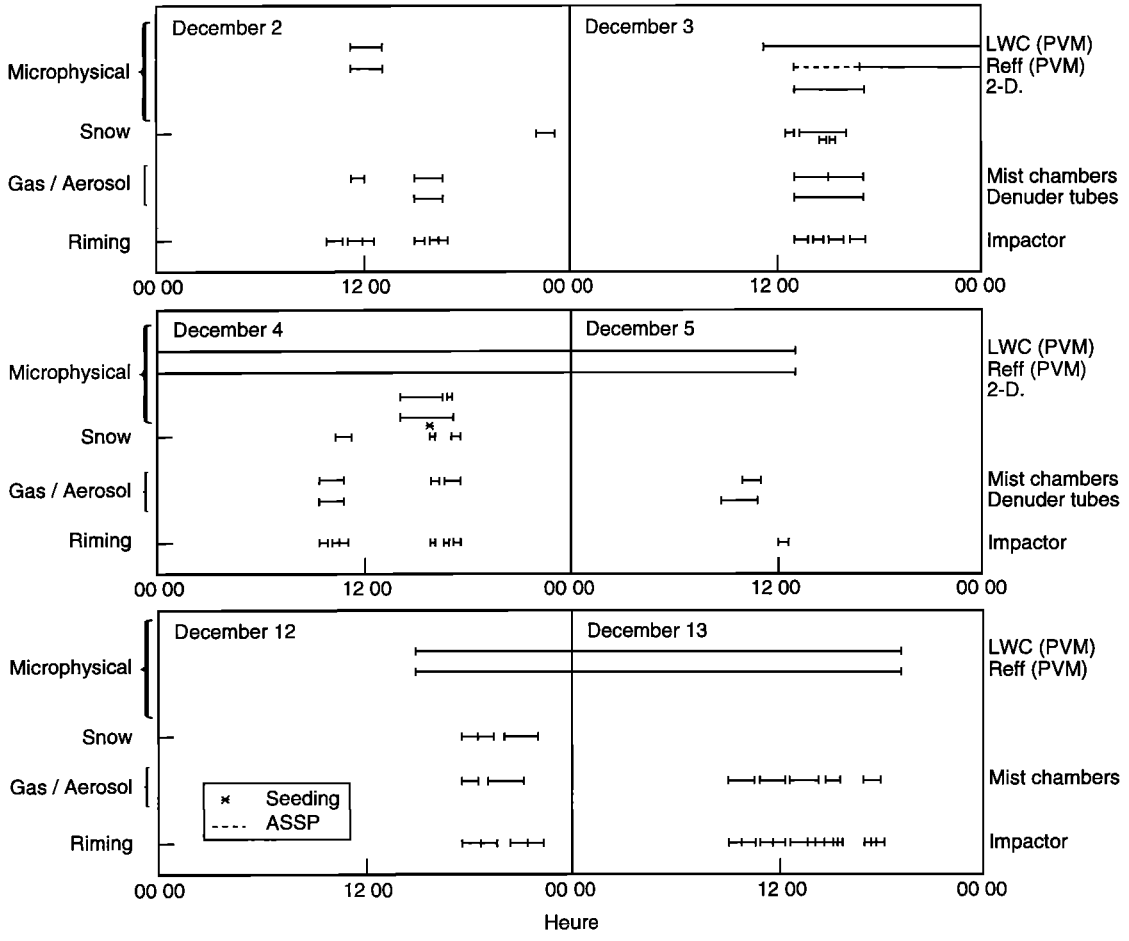

Figure 3. Sampling for chemistry (snowflakes, supercooled liquid water droplets, and interstitial aerosols and gases) and microphysical measurements carried out during events 1 and 2. ASSP, axially scattering spectrometer probe; LWC, liquid water content; PVM, particulate volume monitor.

sampling aerosols, we calibrated its accurate size cut by using a differential mobility particle sizer (DMPS) detecting fine particles in the range of 0.1-0.7 μm diameter [*Reischl,* 1991] and an aerodynamic particle sizer measuring coarse particles (from 0.77 to 3 μm) [*Baron et al.,* 1993]. These measurements were done at the Finnish Meteorological Institut in Helsinki and indicate a collection efficiency of zero for particles larger than 0.8 μm. For particles ranging from 0.1 to 0.7 μm the collection efficiency was 0.5 ± 0.1. Thus in-cloud aerosol sampling downstream from our inertial droplet separator will not be relevant for coarse particles. For particles smaller than 0.7 μm we therefore have assumed that the concentration is twice what we measured, with an uncertainty of 20%.

Soluble gases present in interstitial air were sampled with two mist chambers in series. These mist chambers were downstream from the droplet separator (connection on port B) and a Teflon Millipore FALP (37 mm diameter) filter (Figure 5b). The mist chamber technique was successfully used in sampling HNO_3 and carboxylic acids by *Talbot et al.* [1990], SO_2 by *Klemm and Talbot* [1991], HCl by *Legrand et al.* [1996]. Ammonia was sampled this way as well. The two mist chambers connected in series permit us to investigate the efficiency of the gas trapping. The collection efficiency, defined as the difference of mass trapped between the front chamber and the second chamber divided by the mass collected in the front chamber, was close to 85% for HNO_3, 80% for HCl, 75% for HCOOH, 70% for CH_3COOH, 68% for SO_2, and 76% for NH_3 (Table 1). Because of a possible effect of aerosols impacted on the on-line filter upstream from the mist chambers (decomposition or uptake of gases), two additional gas sampling lines using annular denuder tubes were set up at ports A1 and A2 of the droplet separator (Figure 5b). Each line is made of three identical denuder tubes mounted in series and equipped with a backup teflon filter. In the NH_3 line the tubes are coated with H_3PO_4 [*Rosenberg et al.,* 1988]. In the line for acidic gases the tubes are coated with Na_2CO_3 [*Ferm,* 1986; *Norton,* 1992]. The use of three denuder tubes in series allows us to examine the collection efficiency as well as to detect a possible decomposition of aerosols trapped on the backup filter and a subsequent retrodiffusion of gases on the third coated tube. Collection efficiency, defined as the difference of mass trapped between the front denuder tube and the second denuder tube divided by the mass collected in the first denuder tube, was close to 85% for HNO_3, 96% for HCl,

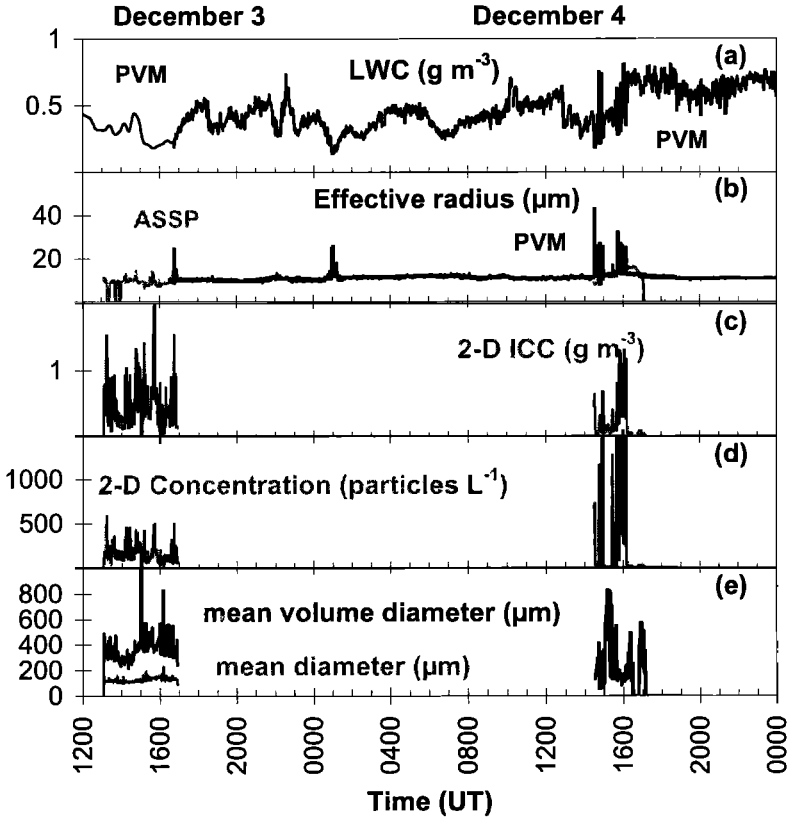

Figure 4. Cloud microphysical parameters measured during event 1. (a) Liquid water content (in g m^{-3}) measured by the PVM 100 device. (b) Effective radius (in μm) of liquid droplets measured by the PVM (solid line) and the ASSP (shaded line). (c) Ice content (ICC)(in g m^{-3}) provided by the two-dimensional optical array probe (OAP 2D). (d) Concentration of ice particles (particles L^{-1}) measured by the OAP 2D. (e) Mean volume (solid line) and mean (shaded line) diameter (in μm) provided by the OAP 2D.

90% for HCOOH, 74% for CH_3COOH, and 90% for NH_3 (Table 1). During the cloud event 1, the mass trapped on the third denuder tube was always lower than the mass trapped on the second denuder tube and was close to the blank value, even for ammonium and nitrate species, suggesting that no significant artifact related to decomposition of aerosols took place under the atmospheric conditions encountered there.

As seen in Table 1, gas concentrations derived from mist chambers and denuder tubes are in good agreement, except for HNO_3 whose levels are 2 times higher in mist chambers than in denuder tubes. Although mist chamber extracts have been kept frozen until analysis, several oxidants (H_2O_2 or O_3) also trapped in mist chambers may have subsequently partly oxidized other NO_y into nitrate. Among NO_y, HNO_2 is the most likely candidate to interfere with nitrate measurements from mist chamber sampling, because of its relatively high solubility. Gas phase HNO_2 measurements inferred from nitrite measurements in both mist chamber and denuder tube extracts indicate significant levels of HNO_2 (882 $\pm$ 648 ng m^{-3} and 820 $\pm$ 335 ng m^{-3} from denuder tubes and mist chambers, respectively). If present in the mist chamber samples, H_2O_2 would be mainly consumed by S(IV) and would not be available to oxidize HNO_2 into nitrate, since the rate constant of the reaction of HNO_2 on H_2O_2 is some 10^4 times lower than the rate constant of the reaction between H_2O_2 and HSO_3^- at 298 K [*Jacob*, 1986]. The rate constant of the reaction S(IV) + O_3 is 5 times higher than the rate constant of the reaction NO_2^- + O_3 [*Jacob*, 1986]. Using the measured S(IV) and sulfate levels present in the mist chamber samples (section 3.4) and given the gas phase concentrations of SO_2 and HNO_2, we can estimate that the oxidation of nitrite into nitrate by ozone may account for 3-50% (16% in average) of the observed nitrate levels in the mist chamber samples. Thus the oxidation of HNO_2 by ozone in the mist chamber samples may have led to a slight overestimation of HNO_3 concentrations of the gas phase. In this paper we have used gas concentrations obtained by using the mist chambers which permit sampling times that are shorter (as low as 20 min) than those of the denuder tubes (2 hours) and mean values when both mist chambers and denuder tubes were operating.

3.3. Rime Collection

Cloud supercooled water droplets were collected as rime by sucking air in a single-stage impactor backed by a large wind shield, as successfully developed by *Kruisz et al.*[1993] for sampling cloud water under high-wind conditions. During the sampling, supercooled cloud droplets are impacted on a stainless steel plate and form a rime deposit. The airflow rate through the inlet (105 m^3 h^{-1}) corresponds to a Reynolds

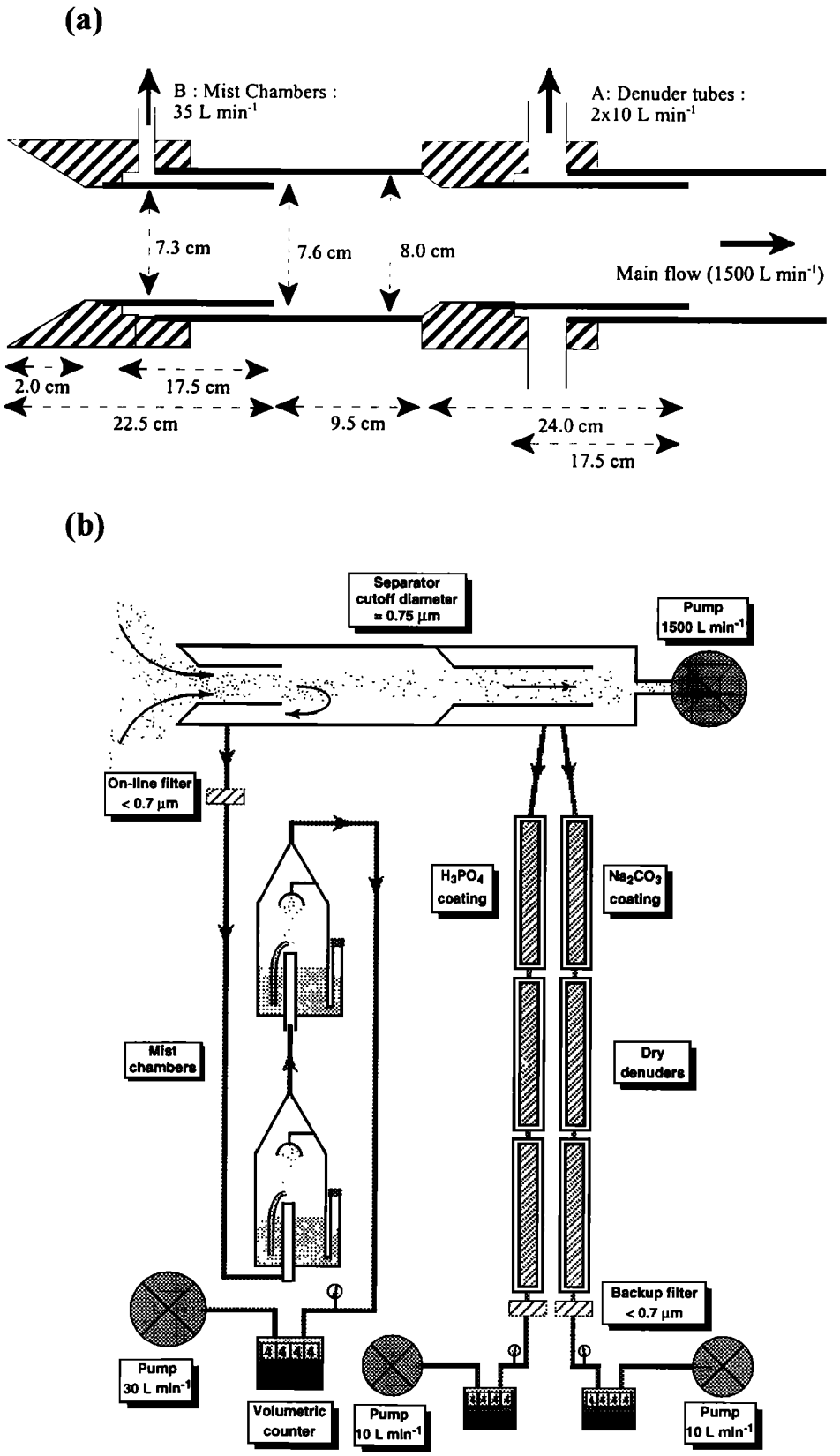

Figure 5. (a) The droplet separator: air enters through the 7.3 cm diameter inlet (left side) with a flow rate of 1500 L min^{-1} (velocity of 6 m s^{-1}). The Reynolds numbers are 26,500 at jet and 470 (laminar flow) at sampling lines (for a flow rate of 30 L min^{-1}). Using these operating conditions, the computed size cut is close to 1.0 μm. (b) Plan view of devices used for sampling of interstitial gases and aerosols.

Table 1. Air Volume Samples, Mean Field Blanks Translated Into Atmospheric Concentrations, Collection Efficiency, Atmospheric Concentrations, and Precision of Determination

Species	Method	Volume of Air Sampled, m^3	Sampling Interval	Field Blank Values, ng m^{-3}	Collection Efficiency, %	Atmospheric Concentrations,[a] ng m^{-3}	Atmospheric Precision, %
NH_3	denuder	2	2 hours	111 ± 22	90 ± 19	107 ± 75 (n = 5)	45 ± 22
	mist chamber	1	20 min	15 ± 10	76 ± 17	142 ± 134 (n = 17)	36 ± 30
						84 ± 46 (n = 5)	
HCl	denuder	2	2 hours	8 ± 5	96 ± 6	88 ± 63 (n = 5)	25 ± 30
	mist chamber	1	20 min	2 ± 3	80 ± 10	94 ± 90 (n = 17)	37 ± 24
						66 ± 19 (n = 5)	
HNO_3	denuder	2	2 hours	10 ± 2	85 ± 7	143 ± 68 (n = 5)	5 ± 2
	mist chamber	1	20 min	4 ± 6	84 ± 7	430 ± 375 (n = 17)	25 ± 27
						305 ± 350 (n = 5)	
HCOOH	denuder	2	2 hours	87 ± 6	90 ± 11	795 ± 270 (n = 5)	5 ± 1
	mist chamber	1	20 min	22 ± 15	75 ± 9	620 ± 345 (n = 17)	16 ± 7
						600 ± 198 (n = 5)	
CH_3COOH	denuder	2	2 hours	120 ± 13	74 ± 19	740 ± 360 (n = 5)	7 ± 3
	mist chamber	1	20 min	35 ± 20	70 ± 7	740 ± 400 (n = 17)	20 ± 21
						986 ± 378 (n = 5)	
SO_2	denuder	2	2 hours	35 ± 10	~70		
	mist chamber	1	20 min	105 ± 29	68 ± 10	1700 ± 1350 (n = 17)	13 ± 12
NH_4^+	Teflon filters	1	20 min	3 ± 2	-	232 ± 288 (n = 17)	25 ± 5
$HCOO^-$	Teflon filters	1	20 min	17 ± 3	-	18 ± 16 (n = 17)	31 ± 5
CH_3COO^-	Teflon filters	1	20 min	11 ± 2	-	12 ± 8 (n = 17)	30 ± 17
Cl^-	Teflon filters	1	20 min	9 ± 1	-	124 ± 106 (n = 17)	22 ± 3
NO_3^-	Teflon filters	1	20 min	5 ± 1	-	210 ± 340 (n = 17)	22 ± 3
SO_4^{--}	Teflon filters	1	20 min	38 ± 8	-	684 ± 940 (n = 17)	22 ± 3
$C_2O_4^{--}$	Teflon filters	1	20 min	1 ± 1	-	6 ± 4 (n = 17)	40 ± 50

Values of field blanks translated into atmospheric concentrations are given ± standard deviation. Atmospheric concentrations are those encountered during cloud events 1 and 2.

For comparison, we report mean atmospheric concentrations inferred from the five mist chambers run simutaneously to the five denuder tubes.

[a] Number of samples is given in parentheses.

number of 8752 and a Stokes number of 0.193. Under these conditions the cutoff diameter of the impactor is close to 8.5 μm. During sampling of supercooled liquid droplets, gases of concern may be incorporated into the ice deposits by vapor deposition. However, because of high LWC values encountered in this study (from 0.18 to 0.8 g m^{-3}, Figure 4) with temperatures ranging from -2° to -9°C, based on the formulae of *Ludlam* [1951], the vapor deposition to rime mass ratio may never exceed 0.1.

3.4. Chemical Analysis

Samples were processed in a field laboratory equipped with clean air bench, ultrapure water Millipore device, and two ion chromatographs (Dionex X100 and X500). Anion measurements were made on a Dionex X500 equipped with an AS11 separator column following working conditions detailed by *Jaffrezo et al.* [1998]. Using a gradient pump system, the eluant (NaOH solution with 8% of methanol) concentration is increased from 0.16 to 16 m*M*, rendering possible the determination of major anions (acetate, formate, chloride, nitrite, nitrate, sulfite, sulfate, and oxalate) as well as many other oxygenated organic ions (succinate, glutarate, malate, pyruvate, glycolate, and lactate). Cation (sodium, ammonium, potassium, magnesium, and calcium) measurements were achieved on a Dionex X100 equipped with a CS 12 separator column using methanesulfonic acid (0.1 *M*) at a flow rate of 1 mL min^{-1}. Analysis of cloud water samples and snowflakes was usually made within 1 hour after sampling. All other sampling including mist chamber and denuder tube extracts as well as aerosol filters were stored in a freezer until analysis.

The aqueous extract of denuder tubes coated with Na_2CO_3 cannot be directly measured with the working conditions reported by *Jaffrezo et al.* [1998], because of the carbonated matrix of samples. This matrix was here removed before analysis by flowing samples at a rate of 1mL min^{-1} through an ion exchange resin (Alltech Maxi-Clean IC/H^+) replacing sodium by proton.

Each mist chamber sampling has been analyzed 2 times. A first aliquot has been directly analyzed for determinations of ammonia, hydrochloric acid, nitric (and nitrous) acids, and formic and acetic acids. Sulfite and sulfate present in this first aliquot were also determined. Initially, the sulfur dioxide is physically trapped in mist chamber water mainly as sulfite. However, because of the presence of oxidants trapped in the mist chamber, the S(IV) can be partly converted into sulfate. The atmospheric SO_2 concentrations have been achieved by measuring the sulfate amount present in a second aliquot of the mist chamber water after the addition of 10 μL per milliliter of sample of H_2O_2 (0.3%) and Na_2CO_3 (0.1 *M*) following *Klemm and Talbot* [1991]. This cannot be applied to determine SO_2 concentrations in cloud water and snow, because the increase of sulfate concentrations due to the SO_2 oxidation is here too small with respect to the amount of sulfate already present in these samples as aerosol sulfates. SO_2 concentrations in cloud water and snow samples were estimated by analyzing sulfite present in samples and assuming that S(IV) present in these samples is mainly related to the presence of SO_2. Note, however, that under our working conditions, the alkaline eluant (NaOH) was found to be able to completely convert $CH_3(OH)SO_3^-$ (hydroxymethanesulfonate (HMSA)) into sulfite.

Table 2. Mean Concentrations in Precipitating Snow and Rimed Ice Deposited in the Fog Impactor During Events 1 and 2

Species	Rimed Ice, ng g^{-1}	Snow, ng g^{-1}
NH_4^+	3912 ± 2933	1027 ± 404
$HCOO^-$	240 ± 198	64 ± 38
CH_3COO^-	270 ± 190	120 ± 78
Cl^-	3090 ± 3328	1560 ± 2296
NO_3^-	23555 ± 26342	4100 ± 1940
SO_4^{2-}	8130 ± 5654	2085 ± 1191
$C_2O_4^{2-}$	73 ± 55	25.8 ± 26.0
S(IV)	114 ± 121	52 ± 59

Mean concentrations are given ± standard deviation. There are 10 samples from precipitating snow and 36 samples from rimed ice deposited in the fog impactor.

The precision of measurements is related to the precision of IC measurements, the collection efficiency, and the blank variability. In spite of a small sampled volume of air (~ 1 m^3), the precision of gas phase measurements with mist chamber sampling typically ranges from 13 to 37 % and is mainly related to blank variability and uncertainty in sampled volume determination (Table 1). Gas phase measurements with denuder tube sampling are sometimes less precise because of a higher variability of blank values, especially for NH_3 determinations. Except in the case of very low oxalate concentrations, aerosol concentrations are well known with typical precision close to 20-30 % mainly related to uncertainty in the measured collection efficiency in the droplet separator (see section 3.2).

Concentration ranges encountered in snow and rimed ice deposited in the fog impactor having occurred during events 1 and 2 are summarized in Table 2. Precision is typically 5-10% for nitrate, ammnonium, and sulfate; 10-20% for chloride, formate, and acetate; and 20-30% for SO_2. Less accurate is the determination of oxalate levels (~30%) for which errors reach 100% when measuring low-content samples.

The pH of samples has been calculated by checking the ionic imbalance between anions and cations mesured by ion chromatograhy, taking into account the partial dissociation of weak acids (formic, acetic, and oxalic acids and SO_2) and ammonia:

$$[H^+] \approx [Cl^-] + [NO_3^-] + [SO_4^{2-}] + [SO_4^{2-}]/(1 + 10^{(pK-pH)}) + [CH_3COO^-]/(1 + 10^{(pK-pH)}) + [HCOO^-]/(1 + 10^{(pK-pH)}) + [C_2O_4^{2-}]/(1 + 10^{(pK-pH)}) + [C_2O_4^{2-}]/(1 + 10^{(pK-pH)}) - [Na^+] - [K^+] - 2 * [Mg^{2+}] - 2 * [Ca^{2+}] - [NH_4^+]/(1 + 10^{(pH - pK)}). \quad (1)$$

The calculated pH values in liquid cloud droplets mainly range from 3 to 4.8, being low enough so that carbonate related to the carbon dioxide dissolution could be neglected. Other anions than the ones considered in equation (1) have sometimes been detected but never represented more than 2 % of the total ionic budget. Precision on calculated H^+ concentrations derives from precision on IC measurements and is typically 20-30%. This corresponds to a precision of 0.1 units at the pH scale.

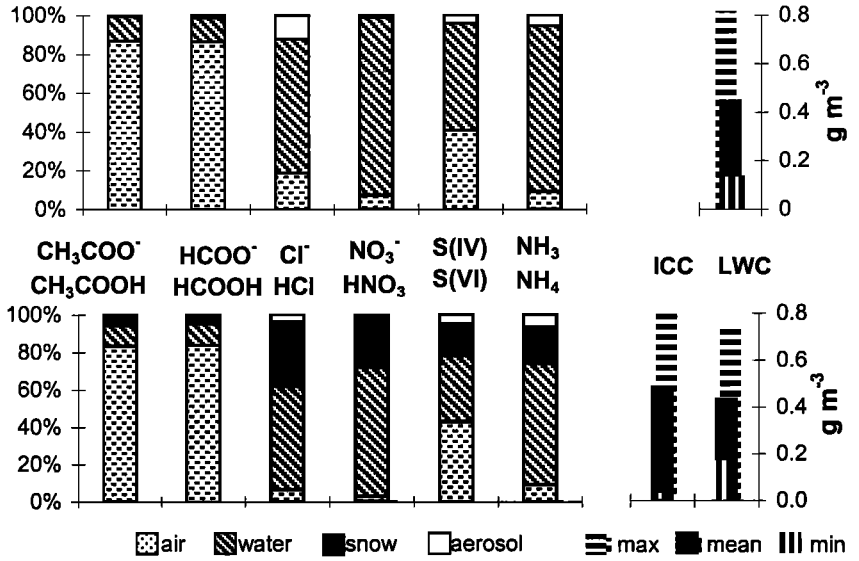

Figure 6. Mean weighted percentages of species present in each phase of the cloud (interstitial aerosol and air, and supercooled water and ice) in (top) clouds without ice and in (bottom) clouds with precipitating ice.

4. Chemical Partition Between Rimed Supercooled Cloud Droplets, Snowflakes, Interstitial Gases, and Aerosols

On the basis of observed concentrations of acetate, formate, chloride, nitrate, ammonium, and sulfur (S(IV) + S(VI)) and on the liquid and ice content of clouds, we have summarized in Figure 6 the weighted percentage of species present in the different phases (interstitial aerosol and gas phases and supercooled water and ice particles). We here have assumed that the chemical composition of a supercooled cloud droplet is identical to the one of rimed ice collected in the fog impactor (see section 4.1.1). This picture clearly points out large differences in the partitioning of chemical species between the condensed water phases and the gas phase. Light carboxylates are mainly present in the gas phase, whereas chloride and nitrate as well as ammonium are mainly present in condensed phases (Figure 6). Sulfur species are present in both the gas phase (as SO_2) and condensed phases (mainly as sulfate: 93-99% in cloud water and 95-99.5% in snow). Comparing the concentrations of various species in snow and water, we can observe that the water to snow ratio is widely variable from one to another event depending on the degree of riming of snowfall (low ratio for heavy rimed snow and high ratio for lightly rimed snow). One can also observe (Figure 7) that lightly rimed snows show a clear difference with high water to snow ratios for mainly aerosol species (sulfate, and oxalate) and weak ratios for mostly gaseous species (weak acids such as formic and acetic) (Figure 7).

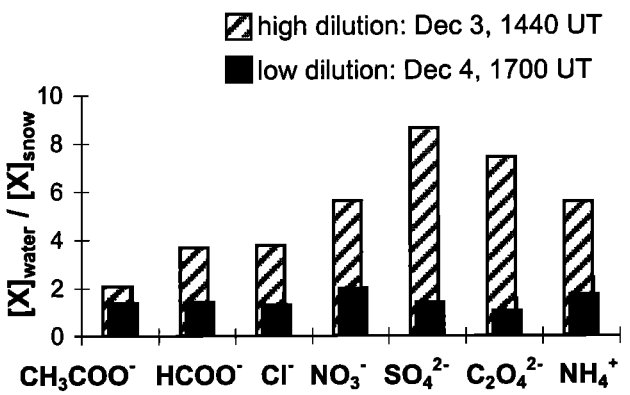

Figure 7. Supercooled water to precipitating ice concentration ratios in two typical cases encountered during event 1: low (high) ratio corresponds to heavy (lightly) rimed snow.

4.1. Equilibrium Between Supercooled Liquid and Gases

Partition of gaseous species between air and droplets in clouds and fogs is usually described in terms of solubility equilibrium, gaseous, and aqueous concentrations of a given species X being related through Henry's law:

$$H^* = [X]_{water} / P_X , \quad (2)$$

where P_X is the partial pressure of species X in the gas phase, $[X]_{water}$ is the total concentration of species X in water, including the possible dissociated or protonated forms in the case of acids and bases, H^* is the effective Henry coefficient, taking into account the influence of pH on the solubility of acids and bases (for a weak monoacid, H^* derives from the usual Henry coefficient H according to $H^* = H\ (1 + K_a/[H^+])$, K_a being the dissociation constant of the acid).

Numerous studies investigating simultaneously gaseous and aqueous concentrations in liquid clouds or fogs have shown that for species such as strong acids as well as weak acids and bases, measured concentrations do not obey Henry's law. In order to quantify the departure from equilibrium, *Winiwarter et al.* [1994] introduced the saturation coefficient (denoted q) as follows:

$$q_X = \frac{[X]_{observed}}{H_X^* P_X} . \quad (3)$$

A saturation coefficient smaller (greater) than 1 corresponds to a liquid phase subsaturated (supersaturated) with respect to the gas phase. It has been evidenced that bulk samples from clouds in which individual droplets are at solubility equilibrium can be either subsaturated or supersaturated. Apparent sub-saturation ($q<1$) occurs when the temporal variability of LWC is important [*Winiwarter et al.*, 1992], and supersaturation occurs when pH varies with droplet size [*Pandis and Seinfeld*, 1991].

4.1.1. Concentration in supercooled droplets. In the following we have used for the concentration of species in supercooled water the concentration in the ice formed as rime in the droplet impactor. This could lead to underestimating the concentrations in supercooled water because of a poor retention of gases in ice during the shock freezing of droplets: gases are less soluble in ice than in water, so that freezing leads to their exclusion from the forming ice to the remaining water. The subsequent increase of gas concentrations in the water eventually leads to outgassing to the atmosphere. The overall process is quantified by the retention coefficient (Γ), which is the ratio of the remaining concentration of gas in the rime to the initial concentration in the supercooled water. The overall retention may depend on the competition between numerous individual kinetics such as the outgassing efficiency at the water-air interface and the solidification speed governed by transfer in the substrate of the latent heat of solidification [*Lehman et al.*, 1999]. The solidification speed may also influence the shape of the growing interface, a dendritic one (fast solidification associated with a good heat transfer out of the growing ice) being a better trap than a planar one (slow solidification) [*Lehman et al.*, 1999]. *Snider and Huang* [1998] suggested an influence of the frequency at which new layers form, the last formed layer being the only one able to degas. One can also suggest an influence of the initial degree of saturation of droplets with respect to the air: in unsaturated droplets, exclusion of gases from the forming ice to the remaining water will first lead to saturating this water before leading to an efficient outgassing. This complex dependence on many different parameters could explain the huge discrepancies in Γ values obtained from laboratory and field studies. *Iribarne and Pyshnov* [1990] showed that no acidity is lost (i.e., a retention coefficient close to 1) as HCl or HNO_3 when droplets freeze by contact with an ice surface at temperatures ranging from -8° to -12°C. For SO_2, laboratory studies indicate a very different retention coefficient from less than 10% [*Lamb and Blumenstein*, 1987] and 60% [*Iribarne et al.*, 1990]. Field measurements of the H_2O_2 retention coefficient suggest values from 0.05 [*Snider and Huang*, 1998] to 0.24 [*Snider et al.*, 1992], which largely differ from the value close to 1 derived from laboratory experiments [*Iribarne and Pyshnov*, 1990].

This possible outgassing has been tested here by sampling gases simultaneously downstream from the cloud impactor (line 1) and in the usual line (line 2) downstream from our droplet separator (port B, see Figure 5a). For the most soluble gases that are mainly in the aqueous phase (more than 90%, see Figure 6), a light outgassing to the atmosphere should be easily detected with concentrations higher in line 1 than in line 2. This has not been observed for HNO_3, HCl, and NH_3. Hence, in the following, we assume a total retention of those gases during freezing in the impactor. For the weak acids, mainly gaseous, this test is not as sensitive: the major mass fraction of these species is already in the gas phase, so that a significant difference between line 1 and line 2 can only result from a very important outgassing during riming. For acetic and formic acids such a difference has not been observed, meaning that the retention of those acids during shock freezing of supercooled liquid cloud droplets is better than 50%. Hence, in section 4.1.2, we have assumed that the retention coefficient of formic and acetic acids is equal to 1. In the case of S(IV), a clear outgassing has been observed, SO_2 concentrations measured in line 1 being systematically higher than those in line 2. The retention coefficient of S(IV) has been calculated as the ratio of the mass difference between line 1 and 2 (outgassed mass of SO_2) to the sum of the remaining mass of S(IV) in frozen water and the outgassed mass of SO_2. This gives a retention coefficient of 2 ± 1 % for S(IV). Since we suspect that a large fraction of S(IV) was present in rimed ice as HMSA (see section 4.2.1), the retention coefficient cannot be compared with the value of Γ obtained by *Lamb and Blumenstein* [1987] for SO_2.

4.1.2. Saturation coefficient in the presence of ice. The Henry coefficients used for the calculation of the saturation coefficient q are summarized in Table 3. It has to be noted that those coefficients are poorly known for carboxylic acids, varying within a factor of 2 from one determination to another. We here chose the most recent experimental values from *Johnson et al.* [1996]. It has to be kept in mind that a change of the Henry constant by a factor of 2 will change the saturation coefficient by the same extent.

Figure 8 indicates departures from the Henry's law equilibrium for all species. One third of the cloud water samples were collected when ice particles were present. Because of the Bergeron process, snow fall induces reevaporation of water droplets and could therefore shift the

Table 3. Henry's Law Coefficients Used for Saturation Coefficient q Calculations

Species	H at 268 K, mol L^{-1} N^{-1} m^2	$-\Delta H^\circ/R$, K	References
CH_3COOH	4.3×10^{-1}	6300	*Johnson et al.* [1996]
HCOOH	8.7×10^{-1}	6100	*Johnson et al.* [1996]
SO_2	3.7×10^{-5}	3100	*Pandis and Seinfeld* [1989]
NH_3	2.9×10^{-3}	4200	*Clegg and Brimblecombe* [1986]
HCl	5.4×10^{2}	9000	*Brimblecombe and Clegg* [1988]
HNO_3	6.1×10^{2}	8700	*Brimblecombe and Clegg* [1988]

The temperature dependence is $H(T) = H(268\ \text{K}) \exp[-\Delta H^\circ/R\ (1/T - 1/268)]$. For HCl and HNO_3 the units are $mol^2\ L^{-2}\ N^{-1}\ m^2$ as the constant takes the total dissociation of those acids into account.

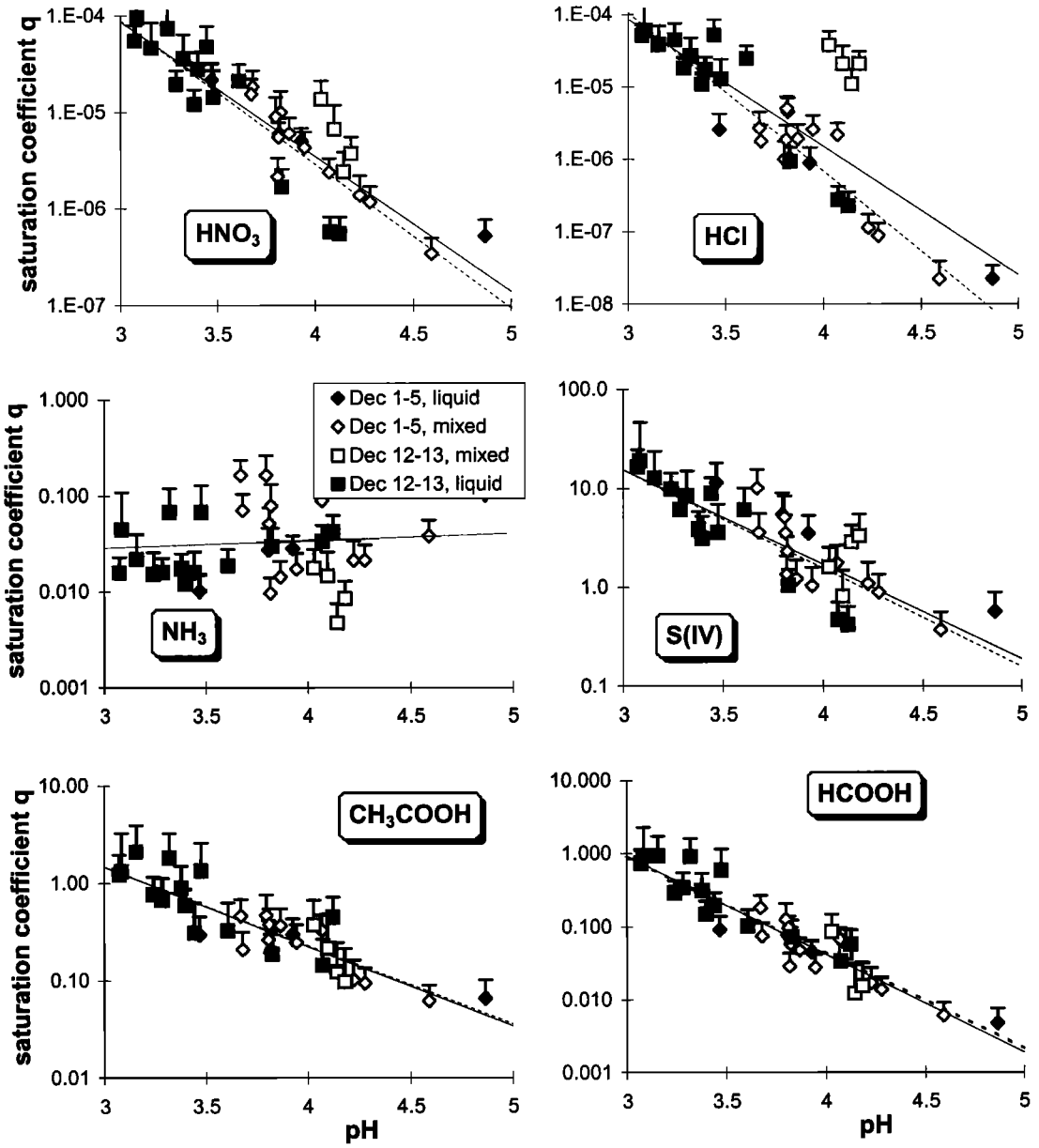

Figure 8. The pH dependence of saturation coefficients q in the liquid phase with respect to the gas phase (see text) for weak and strong acids as well as for ammonia. Solid lines are the regression lines for the entire data sets, and dashed lines are the regression lines excluding measurements in mixed (supercooled water and ice) clouds.

overall partition between air and supercooled water. As depicted in Figure 8, no significant difference can be detected on q values corresponding to the case of mixed (liquid and ice water) clouds with respect to those corresponding to liquid water clouds. This finding suggests that the presence of ice in clouds does not modify the overall partition between air and water. This can be seen as well by comparing the two regressions plotted in Figure 8, the first one only referring to measurements done in supercooled clouds and the second one considering the entire set of measurements. Thus the Bergeron process does not influence the overall partition of soluble gases between air and water, and incorporations of soluble gases in the ice and in water can be considered as uncoupled problems.

Figure 8 shows very large subsaturation of the liquid phase with respect to the gas phase for the most soluble species (HNO_3, HCl, and NH_3) with saturation coefficient q as low as 10^{-6}. The less soluble weak carboxylic acids show weaker departures from the equilibrium, depending on pH and species. In contrast, on the entire pH range the S(IV) content in the liquid phase exhibits a super-saturation with respect to the Henry's law equilibrium of SO_2. As discussed in section 3.4, the measurement of S(IV) in the liquid phase by using ion chromatography includes sulfite as well as HMSA formed from the reaction between S(IV) and HCHO. HMSA has not been determined in the cloud samples collected during this campaign. On the basis of an order of magnitude of HCHO levels expected in this kind of cloud water, we tentatively

Table 4. Ranges of Saturation Coefficients q Observed by Various Authors

Saturation Coefficient q	pH Range	References
	CH_3COOH	
0.01 - 5	3- 7	*Facchini et al.* [1992]
0.01 - 10	3 - 7	*Winiwarter et al.* [1994]
0.01 - 10	3 - 7	*Keene et al.* [1995]
0.01 - 0.6	3 - 5.5	*Laj et al.* [1997]
0.05 - 5	3 - 5	this work
	HCOOH	
0.001 - 2	3 - 7	*Facchini et al.* [1992]
0.003 - 40	3 - 7	*Winiwarter et al.* [1994]
0.01 - 10	3 - 7	*Keene et al.* [1995]
0.1 - 10	3 - 5.5	*Laj et al.* [1997]
0.01 - 1	3 - 5	this work
	SO_2	
0.001 - 10	3 - 7	*Winiwarter et al.* [1994]
0.1 - 10	3 - 5.5	*Laj et al.* [1997]
0.1 - 10	3 - 5	this work
	NH_3	
0.01 - 10	3 - 7	*Facchini et al.* [1992]
0.001 - 1	3 - 7	*Winiwarter et al.* [1994]
0.05 - 0.2	3 - 5	this work
	HNO_3	
R : 0.4 - 1	2 - 7	*Ricci et al.* [1998]
R : 0.6 - 1	3 - 5	this work
10^{-7} - 10^{-4}	3 - 5	this work
	HCl	
10^{-8} - 10^{-4}	3 - 5	this work

For HNO_3, *Ricci et al.* [1998] evaluated the deviation from the equilibrium by calculating the ratio R of the measured to the theoretical solubilized fraction (i.e., the mass present in the liquid divided by the total mass present in the liquid and the gas phases). R cannot be directly compared with the coefficient q used in this study, and for comparison we have also reported R values observed for HNO_3.

examine if HMSA can be the dominant form of S (IV) present in cloud water liquid, thus leading to the observed supersaturation with respect to the Henry's law equilibrium of SO_2. *Munger et al.* [1995] measured HCHO concentrations in cloud water at a rural mountain site close to 9 ± 8 μM. HCHO measurements achieved in mixed clouds present in February 1999 at the Puy de Dôme site indicated levels ranging between 7 and 11 μM [*Houdier et al.*, 2000]. Assuming a typical HCHO level of 10 μM and using the HMSA stability constant of 3.6 10^{6} M^{-1} [*Olson and Hoffmann*, 1989], we calculate that 90% of S(IV) may be present in liquid samples as HMSA. This would largely explain the observed supersaturation of S(IV) in the liquid phase with respect to the Henry's law equilibrium of SO_2. In conclusion, discarding the case of S(IV), all species exhibit a more or less pronounced subsaturation of the liquid phase with respect to the gas phase, as previously found in numerous studies (Table 4).

The subsaturation of the liquid with respect to the gas phase may be due to an overestimation of gas phase concentrations. Although the presence of HNO_2 may have led to an overestimation of HNO_3 levels in the gas phase, this cannot explain the observed subsaturation of the liquid phase by 4-6 orders of magnitude with respect to the gas phase. *Pandis and Seinfeld* [1991] demonstrated that the mixing of droplets in equilibrium at different pH may lead to an apparent supersaturation up to a factor of 3 of the sampled bulk liquid. Conversely, *Winiwarter et al.* [1992] showed that variations of the liquid water content during sampling would lead to a subsaturation by a factor of 5 of the sampled bulk liquid although droplets are originally in equilibrium. However, subsaturations of the liquid phase we observed are also far too important to be explained by the LWC variability and the related bulk sampling artifact pointed out by Winiwarter et al.

For all acidic species, regardless of the mean value of q, the saturation coefficient is strongly dependent on the pH, with correlation coefficients exceeding 0.9 in the linear regression between pH and log(q). This strong dependence on the sample's pH cannot be explained by the sampling artifacts pointed out either by *Winiwarter et al.* [1992] or by *Pandis and Seinfeld* [1991] and suggests that even for the weak acids these departures from theoretical equilibrium are real. The dependence on pH of the departure from equilibrium has been previously discussed by *Winiwarter et al.* [1994] in terms of mass transfer limitations at the water-air interface. Assuming that the departure from equilibrium is mainly caused by such a process, the calculated saturation coefficient q in a droplet of radius a after a lifetime t_f in the cloud can be expressed as:

$$q = \left[\exp\left(t_f \frac{3/4\,\alpha\, v L}{44600\, R T a}\right) - 1\right] \frac{44600}{L H^*}, \qquad (4)$$

where α is the sticking coefficient of the gas on water, v is the mean molecular speed, L is the liquid water content of the cloud, and H^* is the effective Henry coefficient.

Following this theory, the pH dependence of the saturation

Table 5. Scavenging Coefficient of Interstitial Aerosols by Snowflakes and Maximum Contribution of Interstitial Aerosol Impaction to Snow Concentrations Calculated From the Size Distribution of Ice Crystals Assuming an Interception Mechanism During Four Different Snow Events During Which Different Water Liquid and Ice Contents Were Present in the Cloud

	Dec. 3, 1440 UT	Dec. 3, 1500 UT	Dec. 4, 1540 UT	Dec. 4, 1700 UT
LWC, g m^{-3}	0.31	0.15	0.43	0.62
ICC, g m^{-3}	0.82	0.43	0.64	0.05
K, 10^{-3} m^3 g^{-1}	2.8	3.2	1.8	3.9
Contribution of aerosol, %	< 0.3	< 0.5	< 0.1	< 0.3

K is the scavenging coefficient of interstitial aerosols by snowflakes. See equation (A4) in the appendix. LWC, liquid water content; ICC, ice content.

coefficient q would be similar to the one of the effective Henry coefficient H^*, suggesting that for strong acids such as HCl and HNO_3 a linear relation between log(q) and pH is expected:

$$\log(q) = A - \mathrm{pH}\,. \tag{5}$$

The theoretical slope for strong acids may therefore be unity and differs from the observed ones (-2.2 ± 0.5 for HCl, and -1.5 ± 0.3 for HNO_3). This strongly suggests that mass transfer limitation is not the only cause for the observed discrepancies. Furthermore, to explain the magnitude of observed sub-saturations, this theory would imply values as low as 0.001 for sticking coefficients α whereas values of α for HNO_3 on water are close to 0.1 (i.e., 100 times higher) [*Ponche et al.*, 1993]. For carboxylic acids the theoretical dependence of log(q) on pH calculated by assuming mass transfer limitations at the water-air interface is not linear, whereas the observations clearly show a linear relation. Furthermore, *Jayne et al.* [1991] measured a sticking coefficient α close to 0.1 for those gases, which leads to subsaturation of the liquid phase only for a droplet's lifetime smaller than 1 s.

In conclusion, although the mass transfer limitation in achieving interfacial equilibrium between air and liquid droplets may partly account for the observed subsaturation, other processes such as a chemical destruction of these species in cloud water need to be investigated. It has to be noted that the very high subsaturations observed for the most soluble species (HNO_3, HCl, and NH_3) are likely the main reason for the very good retention of those species observed during freezing of the supercooled droplets in the impactor (section 4.1.1): the water being subsaturated, the segregation that takes place at the solidification interface during freezing cannot lead to a sufficient supersaturation in the water phase for an efficient outgassing to the surrounding atmosphere.

4.2. Chemical Composition of the Solid Phase

As depicted in Figure 1, impurities can be incorporated into ice particles by freezing of supercooled droplets on ice crystals (riming process), by condensation of gases during the growth of ice crystals by water vapor diffusion, and by direct uptake of interstitial aerosols and gases onto the ice surface.

For species X only present in aerosols, their concentrations ($[X]_{snow}$) in the mass of ice crystals (m_{snow}) are linked to the mass of X contained in rimed ice accreted on snowflakes (m^X_{rime}) and the mass of X present in interstitial aerosols taken up by ice particles ($m^X_{aerosol}$):

$$[X]_{snow} = (m^X_{rime} + m^X_{aerosol})/m_{snow}\,. \tag{6}$$

Introducing the rime mass fraction R and the scavenging coefficient of interstitial aerosols by snowflakes (K), equation (6) becomes

$$[X]_{snow} = m^X_{rime}/m_{snow} + m^X_{aerosol}/m_{snow}$$
$$= R\,[X]_{rime} + KC^X_{aerosol}\,, \tag{7}$$

with $R = m_{rime}/m_{snow}$ and $KC^X_{aerosol} = m^X_{aerosol}/m_{snow}$. Value m_{rime} is the mass of rime accreted on the snow crystal during its fall, so that R is the rime mass fraction of the collected snow and $[X]_{rime}$ is the concentration of X in the rime formed on the crystal by shock freezing of impacted supercooled droplets.

Given the observed size distribution of ice particles, the scavenging of aerosols by ice particles (K) can be calculated by assuming a capture by interception as detailed in the appendix (equation (A4)). For the four snow events summarized in Table 5 the calculated K values range from 1.8 to 3.9x10^{-3} m^3 g^{-1}, and the interstitial aerosol intercepted by ice particles contributes at the best 0.5% of the observed concentrations in snow. Hence equation (7) becomes simpler and suggests that the rime mass fraction R can be estimated by the ratio of the concentrations of X in rime to snow following

$$[X]_{snow} = R\,[X]_{rime}\,. \tag{8}$$

Equation (8) can be applied to species mainly present in the aerosol phase. It is likely applicable to the case of oxalate. However, as previously mentioned in section 3.4, large uncertainties are encountered in determining its concentrations in snow when present at low levels. Sulfate whose concentrations are larger (see Table 2) and accurately determined in both rimed ice and snow is here used to estimate R values by applying equation (8). Finally, equation (8) can also be applied to ammonium since, at least during snow events having occurred on December 3 and 4, ammonia concentrations in the gas phase were very low (Figure 6). As seen in Figure 7, R values calculated by applying equation (8) to oxalate, ammonium, and sulfate are in good agreement, fluctuating from less than 2 on December 3 to more than 6 on December 4.

The rime mass fraction R can be calculated in the same manner as the scavenging coefficient K from the size distributions of both

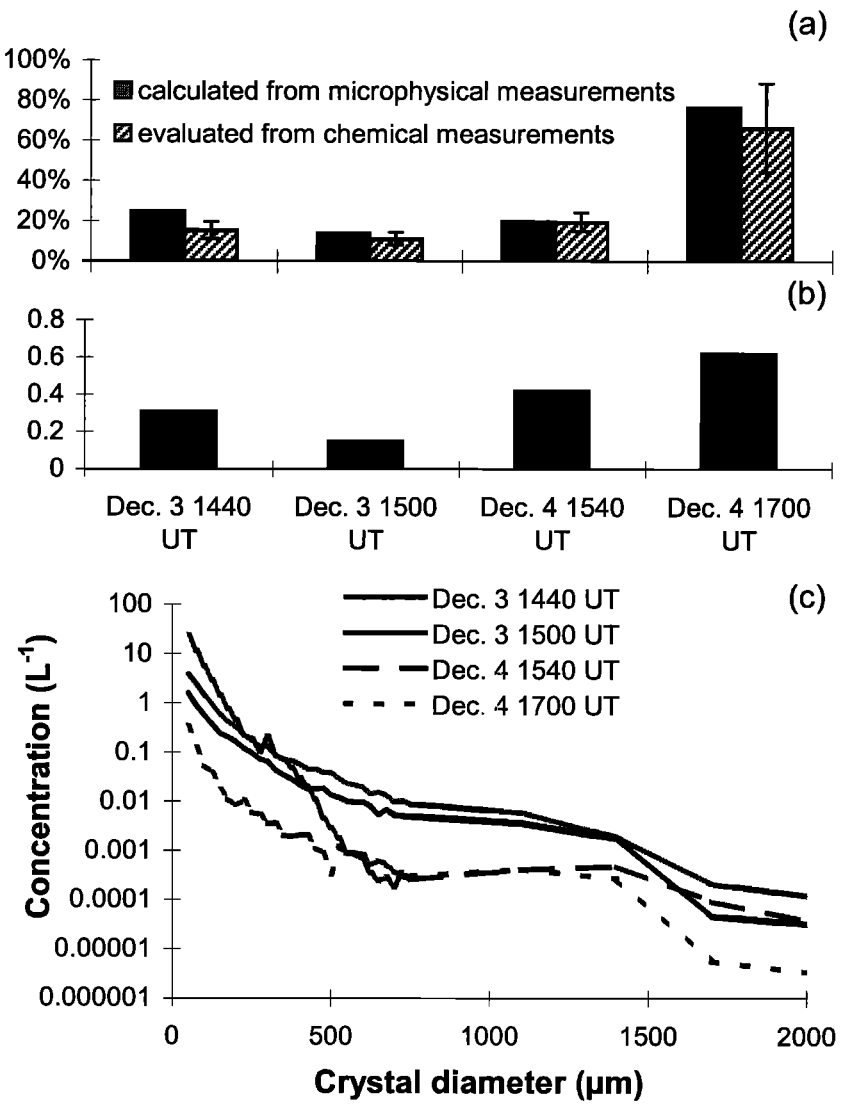

Figure 9. (a) Rimed mass fraction of snowflakes calculated assuming an interception mechanism (see equation (A5) in the appendix) and estimated from the dilution of aerosol species between snow and supercooled water (equation (8)). (b) Liquid water content. (c) Ice particle size spectra.

droplets and ice particles (see equation (A5) in the appendix). Calculated R values and those estimated by applying equation (8) to oxalate, ammonium, and sulfate concentrations in rime and snow are compared in Figure 9. During the four snowfalls that occurred during event 1, the rime mass fractions from the two calculations are very consistent, fluctuating from 15 to 75%. The large increase of the rime mass fraction from December 3, 1500 UT (~15%), to December 4, 1700 UT (~75%), is related to the increase of the liquid water content as expected from equation (A5). For December 4 the large change of R values calculated from the microphysical data from 1540 to 1700 UT is well depicted by applying equation (8) (Figure 9). Such a fast variation of the rime mass fraction is related to the rapid change in the size distribution of ice particles with more small ice particles at 1540 UT than at 1700 UT, while the liquid water content remained unchanged. Thus, applied to aerosol-derived species, equation (8) permits a correct estimation of the rime mass fraction of snowflakes.

For gases, equation (8) remains valid but has to be completed with $[G]_{\text{diffusion}}$, the concentration of gaseous species G that has been incorporated during the growth of the crystal by water vapor diffusion, thus becoming

$$[G]_{\text{snow}} = R\,[G]_{\text{rime}} + [G]_{\text{diffusion}}. \quad (9)$$

4.2.1. Contribution of riming to gases scavenging by ice. The contribution of riming to gases' incorporation in ice crystals depends on the retention during shock freezing, which is very poorly known as discussed in section 4.2.1. Since supercooled droplets are collected as rime in an impactor, we do not have to know the retention coefficient of gases during the riming of snow crystals. To estimate $[\Gamma]_{\text{rime}}$, we use $[\Gamma]_{\text{impactor}}$ and thus have to compare the two retention coefficients: impaction at a fast rate on a metal plate (i.e., the impactor) and impaction at a lower rate on ice crystals. *Lehman et al.* [1999] pointed out that impaction on metal should lead to a better retention than impaction on ice does,

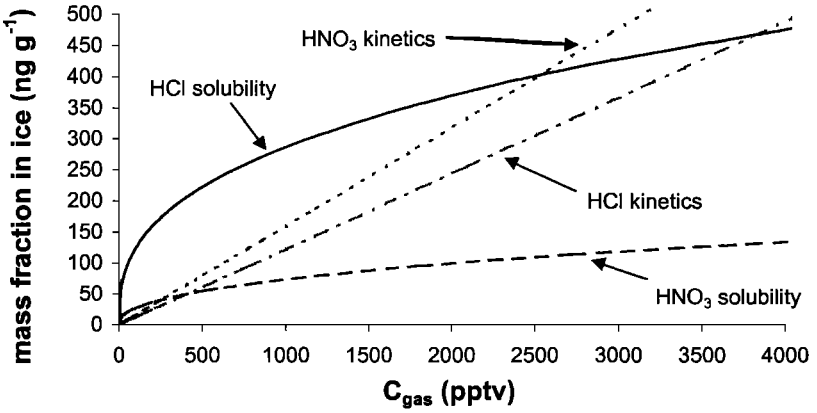

Figure 10. Concentrations of HCl and HNO_3 in ice assuming a cocondensation mechanism (kinetics) and thermodynamic equilibrium (solubility in ice). pptv, parts per trillion by volume.

because of a better heat evacuation leading to a faster solidification. However, this may be valid for a single layer of impacted droplets. When sampling rime in the impactor, the rime sample is usually thicker than a few millimeters. Under these sampling conditions, most of the time, the impaction substrate is therefore ice and not metal. Thus the nature of the impaction substrate (metal rapidly covered by ice in the impactor and ice of snowflakes) may not be here a sensitive parameter influencing Γ values. Layers form at rates varying from 50 to 1000 layers per second in the impactor whereas on the sampled precipitating ice crystals, a second layer is never formed. This difference is in favor of a better retention in the impactor than on snow [*Snider and Huang*, 1998].

In conclusion, although various parameters can modulate the retention coefficient, it is likely that $[\Gamma]_{impactor}$ represents an upper limit for $[\Gamma]_{rime}$. The departure of these two values is expected to be low for species being close to equilibrium with the surrounding atmosphere (i.e., formic and acetic acids).

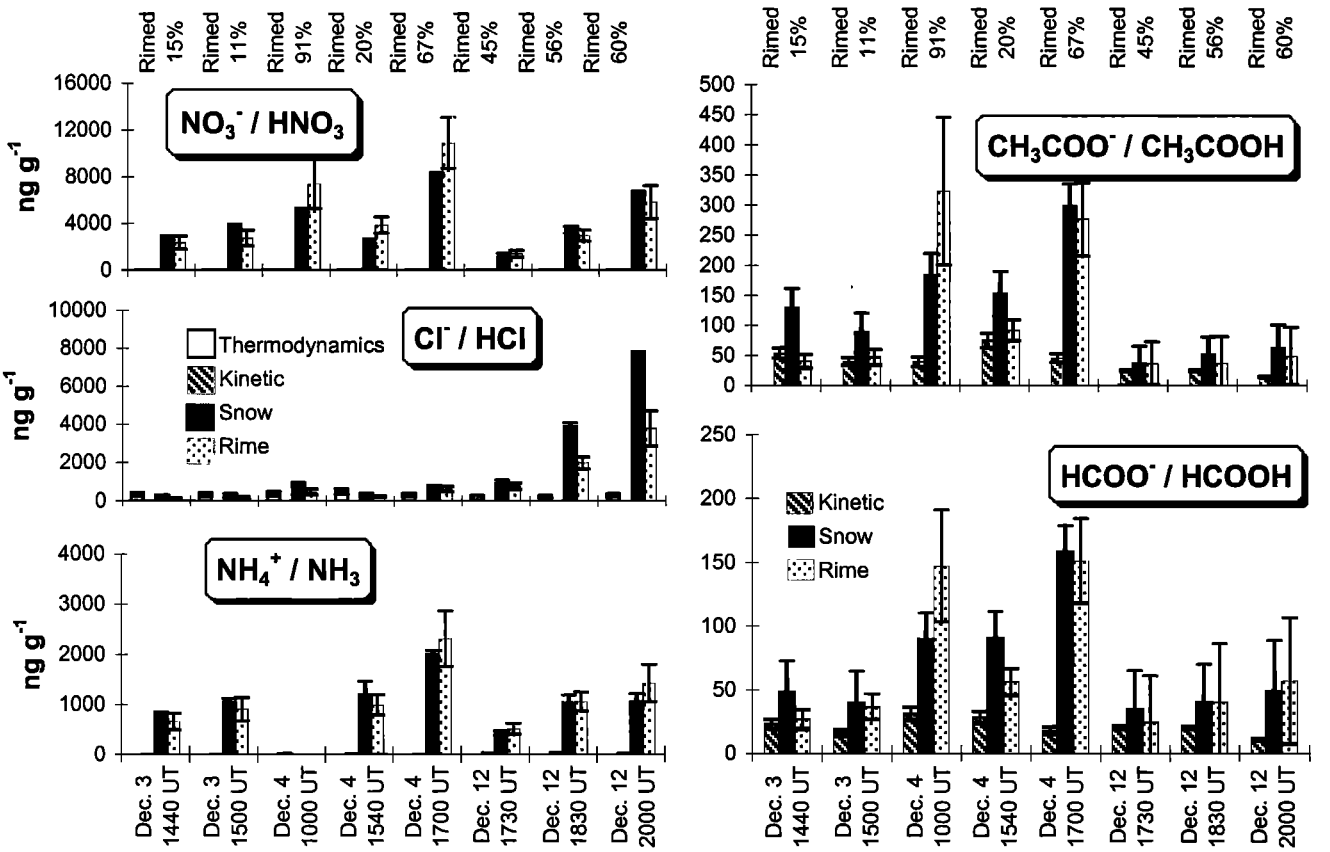

Figure 11. Snow concentrations and contributions of various scavenging mechanisms for gases. The rime contribution calculated here is an upper limit (see section 4.2.1). For HCl and HNO_3 the solubility at equilibrium with the surrounding atmosphere has been calculated as well as the contribution of a cocondensation mechanism.

4.2.2. Incorporation of gases during diffusional growth of ice. During the diffusional growth of ice, trace gases can be adsorbed on the ice surface and subsequently diffuse into the ice volume. They can also be directly incorporated into the ice lattice along with water vapor molecules. The precise mechanisms involved are not well known for the ice. *Dominé and Thibert* [1996] recently suggested that the amount of gases incorporated into ice during its growth is dependent on the equilibrium solubility and diffusion rates of gases in ice as well as the conditions encountered during the ice formation (growth rate of ice).

The mechanism proposed by *Dominé and Thibert* [1996] lies between a kinetic process and a thermodynamic equilibrium. In a cocondensation mechanism (kinetics) the concentration of gases in the ice is given by the ratio of sticking collisions of trace gas on the ice:

$$[G]_{\text{cocondensation}} = \frac{P_G\ \alpha_G}{P_{H_2O}\ \alpha_{H_2O}} \sqrt{\frac{M_G}{M_{H_2O}}}, \qquad (10)$$

where [G] is the mass fraction of gas G in the ice, P is the partial pressure of the considered gas, α the sticking coefficient of gas on ice, and M is the molar mass of the gas.

The value of the sticking coefficient on ice is known for water ($\alpha = 0.5$ at 258 K [*Haynes et al.*, 1992]), HCl ($\alpha = 0.2$ at 258 K), and HNO_3 ($\alpha = 0.2$ at 258 K) [*Dominé and Thibert*, 1996]. For light carboxylic acids, sticking coefficients are not known on ice, and values on water ($\alpha = 0.1$ for HCOOH and $\alpha = 0.15$ for CH_3COOH) have been measured by *Jayne et al.* [1991] between 260 and 290 K.

Whatever the incorporation's mechanism and its kinetics, there will be an equilibrium between ice volume and the surrounding air, governed by energetic consideration. Only for HNO_3 and HCl are solubilities in the ice known [*Thibert and Dominé*, 1997; *Thibert*, 1996]:

$$[HCl] = 1.24\text{x}10^{-10}\ e^{\frac{2806.5}{T}}\ P_{HCl}^{\frac{1}{2.73}}, \qquad (11)$$

$$[HNO_3] = 8.30\text{x}10^{-12}\ e^{\frac{3532.2}{T}}\ P_{HNO_3}^{\frac{1}{2.3}}, \qquad (12)$$

where concentrations are given in g g^{-1} and partial pressures P are given in pascals.

For any gas the kinetics depends linearly on the gas partial pressure while the thermodynamics depends on a power (< 1) of the partial pressure. Hence, at high partial pressures, solubility limits the scavenging during diffusional growth, whereas at low partial pressures, kinetics is a limiting factor, so that other contributions such as surface concentration may be important as well. As depicted in Figure 10, the encountered concentrations of HCl and HNO_3 (Table 1) are well below that limit.

4.2.3. Discussion of the composition of snow in soluble gases. Figure 11 sums up the contributions of riming and incorporation during diffusional growth as detailed in section 4.2.2 and assuming that snowflakes have been formed in a similar environment. This last assumption cannot be directly tested since gas phase and liquid water samples have been collected at 1450 m elevation, while calculations indicate that the snowflakes we collected have been formed at some 1000 m higher elevation. Note that during event 1, vertical soundings indicate that the cloud enveloped the site between 800 and 3000 m elevation. A clear difference appears in the behavior of strong acids and ammonia on one hand and weak acids on the other. For strong acids as well as NH_3, the rime contribution explains the observed concentrations in snow. These three species are highly soluble in water in the range of pH encountered in liquid water collected during events 1 and 2 (most pH values ranging between 3 and 4.3). Therefore the remaining concentrations in the gas phase are very low, rendering the cocondensation contribution negligible and making riming the only efficient mechanism for scavenging these species into ice. In all collected snows the riming contribution largely exceeds the equilibrium concentration calculated from the observed gas phase concentration and the solubility equilibrium of HNO_3 (equation (12)), whereas snows are supersaturated in HCl (equation (11)) only for the most rimed snows. Thus, after deposition of snowflakes at the ground, HNO_3 could hereafter be reevaporated to the atmosphere during the aging of the snow cover.

Riming remains the most important process for incorporating weak acids in snow, but here, cocondensation can clearly be a competitive mechanism, as those species are less soluble in water and have larger concentrations in the gas phase. Furthermore, because these species exhibit high concentrations in the gas phase, thermodynamics (instead of kinetics) may limit the incorporation (see Figure 10). This latter hypothesis is difficult to verify since the solubility of these weak acids is totally unknown in the ice.

Solubility in water thus appears to be the driving characteristic in determining the prevailing incorporation mechanism in snow of mixed clouds. For highly soluble species (here HCl, HNO_3, and NH_3), subsaturation of the supercooled droplets leads to a good retention in rime, and very low concentrations in the gas phase make incorporation during diffusional growth a negligible process: riming is the leading incorporation process. For less soluble species (formic and acetic acids) the water droplets are closer to saturation, so that retention in rime is probably not as good, and gas phase concentrations remain high, making incorporation during diffusional growth a competitive process.

5. Conclusions

In-cloud experiments were carried out at the Puy de Dôme mountain in winter when mixed clouds enveloped the site and snowfalls often occurred. This first comprehensive study of various acidic species present in the three phases (gas, liquid, and ice) of mixed clouds permits us to discuss the processes driving the transfer of various gaseous species (HCl, HNO_3, HCOOH, CH_3COOH, and NH_3) from the atmosphere into precipitation.

As already demonstrated in previous studies, large pH-dependent deviations from theoretical Henry's law equilibrium between liquid and gas phases are seen for all acidic species. This observation remains valid even when ice particles were present. A large subsaturation of supercooled liquid is observed for strong acids, which is only partly explained by a mass transport limitation in achieving interfacial equilibrium between air and liquid droplets. A large supersaturation of S(IV) with respect to the SO_2 equilibrium is observed, likely due to the presence of HMSA in water clouds.

The rime mass fraction of snowflakes calculated from the size distribution of both droplets and ice particles by assuming a droplet capture by interception is very consistent with the one estimated from the observed difference in concentrations of aerosol species (oxalate, ammonium, and sulfate) in liquid water and ice particles.

The retention of gases during the shock freezing of supercooled droplets onto ice particles remains a difficult question. By conducting measurements of gases behing the fog impactor, we can conclude that HCl, HNO_3, and NH_3 were well retained during shock freezing while an outgassing of SO_2 is clearly seen.

For the four snow events examined here the rime mass fraction ranged from 15 to 75%. Under these conditions, rime is found to be the major incorporation process leading to the final composition of snowflakes for HCl, HNO_3, and NH_3. For these highly soluble species the direct incorporation by diffusion from the gas phase during the growth of ice remains limited owing to the low concentrations in the gas phase. In contrast to the case of HCl, the amount of HNO_3 incorporated into snowflakes by the riming process was always found to exceed the equilibrium between the gas phase and the ice phase. That would imply an important change of the nitrate concentration in snowflakes after deposition. For less soluble species such as carboxylic acids the rime contribution is decreased, because of higher concentrations in the gas phase permitting direct incorporation.

Further work is needed to investigate parameters controlling the retention of less soluble species during the shock freezing of supercooled droplets onto ice particles. More laboratory experiments are urgently needed to quantify sticking coefficients of gases on ice as well as equilibrium solubility, which are only known at present for HCl and HNO_3. Finally, both field and laboratory studies need to be extended to other key atmospheric species such HCHO. Such studies are strongly needed in providing a more realistic approach of the role of clouds in modeling the tropospheric chemistry.

Appendix

The rime mass fraction R and the scavenging coefficient of aerosol by snowflakes K can be calculated from microphysical parameters of clouds. Basically, precipitating snow is sampled by intercepting a vertical flux of ice crystals. Thus, for snow collected during a time interval Δt on a surface S, we can write

$$\frac{m^X_{aerosol}}{m_{snow}} = \frac{\Delta t\ S \int_0^\infty n(D) m^X_{aerosol}(D) V_\infty(D) dD}{\Delta t\ S \int_0^\infty n(D) m(D) V_\infty(D) dD}, \quad \text{(A1)}$$

where $n(D)$ represents the concentration of ice particles of diameter (largest dimension) D, $V_\infty(D)$ is the terminal velocity of the ice particle, $m(D)$ is the mass of the ice particle, and $m^X_{aerosol}(D)$ is the mass of the ice particle coming from intercepted aerosol.

Depending on the relative sizes of aerosol and ice particles, the mass of interstitial aerosol collected by ice crystals ($m^X_{aerosol}(D)$) is driven by three different capture mechanisms including diffusion, interception, and inertia. Given the relative size of aerosols and ice crystals, we here only consider the aerosol capture by interception. The mass of X present in aerosol collected by an ice crystal of diameter (largest dimension) D during its lifetime (τ) within the cloud can be expressed as

$$m^X_{aerosol}(D) = \int_0^\tau E_a(D) A(D) V_\infty(D) C^X_{aerosol} dt, \quad \text{(A2)}$$

where $E_a(D)$ is the collection efficiency of aerosols of diameter a by ice particles of diameter D, $A(D)$ is the ice particle cross section area, and $C^X_{aerosol}$ is the mass concentration of aerosol X in the air (g m^{-3}).

Song and Lamb [1991] measured a collection efficiency of 0.006 for ice particles having diameters lower than 300 μm. Ice particles present during our investigation were generally larger than 300 μm, and we here have preferred to apply the theoretical relationship linking the collection efficiency to the diameter of aerosol (a) and ice particle (D) established by *Fuchs* [1964]: $E_a(D) = 3a/D$ (a and D expressed in micrometers). Because here the size distribution of interstitial aerosols is unknown, we have arbitrarily used a value of 2 μm for a in calculating $E_a(D)$. Note that this value is an upper limit for the diameter of the interstitial aerosol and will clearly lead to an overestimate of the mass of submicronic aerosol collected by ice particles. Empirical relationships have been established to relate the terminal velocity and the cross section area of ice particles to their diameters [*Locatelli and Hobbs*, 1974]. Such relationships depend on the form of ice crystals of concern. Given the shape of ice particles seen by the OAP 2D, we have applied the following relationships:

$$A(D) = 0.6495\, D^2$$

$$V_\infty(D) = 1.6834\, D^{0.217},$$

where D is expressed in meters and $V_\infty(D)$ is expressed in meters per second. Assuming a mass growth rate of ice crystals by vapor diffusion of 3.2×10^{-8} g s^{-1} in a cloud at -8°C at 850 mbars (i.e., typical surface conditions encountered during our study) [*Pruppacher and Klett*, 1997], the lifetime of an ice particle of diameter D in the cloud is equal to its mass divided by the mass growth rate. Assuming that the mass (expressed in kilograms) of a crystal of diameter D (expressed in meters) is equal to 0.3584 $D^{2.2}$ [*Locatelli and Hobbs*, 1974], it comes that τ (expressed in seconds) is equal to $1.12 \times 10^{10} D^{2.2}$. This estimation of τ represents an upper limit since the growth rate by vapor diffusion may be higher at a higher elevation where cooler temperatures and lower pressures take place. Note also that the rime process will also decrease the calculated τ value. Hence equation (A1) becomes

$$\frac{m^X_{aerosol}}{m_{snow}} = \frac{\int_0^\circ n(D) V_\infty(D) \int_0^\tau E_a(D) A(D) V_\infty(D) C^X_{aerosol} dt\, dD}{\int_0^\infty n(D) m(D) V_\infty(D) dD}. \quad \text{(A3)}$$

Because of the growth of ice crystals during their fall, D is therefore time dependent. The numerical treatment of equation (A3) is the following

$$\frac{m^X_{aerosol}}{m_{snow}} = \frac{\sum_i \sum_{j=1}^{i} n_i\ V_{\infty,i} V_{\infty,j}\ A_j\ E_{a,j} \tau_j'}{\sum_i n_i\ m(D_i) V_{\infty,i}} C^X_{aerosol} = K_{aerosol} C^X_{aerosol}, \quad \text{(A4)}$$

where $\tau_j' = \tau_j - \tau_{j-1}$.

The total mass of X collected by collision between ice crystals and interstitial aerosols is obtained by applying equation (A4) over the entire size spectrum of ice particles: The concentration of ice particles (n_i) is provided by the channel "i" of the OAP 2D. The probe counts ice particle concentrations as a function of particle diameter (largest dimension) by channels of 25 μm interval between 50 and 800 μm. Four additional channels extend the size range between 700 and 2000 μm diameter.

On the basis of the microphysics of clouds, the rime rate can also be evaluated by using an approach similar to the one previously applied to evaluate the scavenging of interstitial

aerosols by ice particles:

$$R = \frac{\int_0^\infty n(D)V_\infty(D)\int_0^t E(a,D)A(D)V_\infty(D)\mathrm{LWC}\,dt\,dD}{\int_0^\infty n(D)m(D)V_\infty(D)dD} \quad \text{(A5)}$$

In contrast to the collection of aerosols, the collection efficiency $E(a,D)$ of liquid droplets is very dependent on the size distribution of both droplets (diameter a) and ice particles (diameter D). The numerical treatment of equation (A5) has been achieved by using theoretical dependence of the collection efficiency on a and D proposed by *Pruppacher and Klett* [1997]. Because the PVM only provides the effective diameter of liquid droplets and the liquid water content, we have here assumed that the size distribution of droplets is lognormal with a ß value of 0.36, typical for continental clouds [*Chaumerliac et al.*, 1987].

Acknowledgments. The authors want to gratefully thank Susanne Preunkert for assistance in the field, as well as Jean-Marc Pichon, René Hervier, and Wolfram Wobrock for handling of microphysical data. Funding for the experiment was provided by the PNCA program of the French National Research Center (CNRS). We also would like to thank P. Laj (at LaMP) for fruitful discussions and the two reviewers for constructive comments.

References

Baron, P.A., M.K. Mazumder, and Y.S. Cheng, Direct-reading techniques using optical particle detection, in *Aerosol Measurement: Principles, Techniques and Application*, edited by K. Willeke and P.A. Baron, pp. 381-409, Van Nostrand Reinhold, New York, 1993.

Borys, R.D., E.E. Hindman, and P.J. Demott, The chemical fractionation of atmospheric aerosol as a result of snow crystal formation and growth, *J. Atmos. Chem.*, *7*, 213-239, 1988.

Brimblecombe, P., and S.L. Clegg, The solubility and behaviour of acid gases in the marine aerosol, *J. Atmos. Chem.*, *7*, 1-18, 1988.

Chaumerliac, N., E. Richard, J.P. Pinty, and E.C. Nickerson, Sulfur scavenging in a meso-scale model with quasi-spectral microphysics: Two-dimensional results for continental and maritime clouds, *J. Geophys. Res.*, *92*, 3114-3126, 1987.

Clegg, S.L., and P. Brimblecombe, Solubility of ammonia in liquid water and generation of trace levels of standard gaseous ammonia, *Atmos. Environ.*, *20*, 565-570, 1986.

Dominé, F., and E. Thibert, Mechanism of incorporation of trace gases in ice grown from the gas phase, *Geophys. Res. Lett.*, *23*, 3627-3630, 1996.

Dye, J.E., and D. Baumgardner, Evaluation of the forward scattering spectrometer probe, part 1, Electronic and optical studies, *J. Atmos. Oceanic Technol.*, *1*, 329-344, 1984.

Facchini, M.C., et al., Phase-partitioning and chemical reactions of low molecular weight organic compounds, *Tellus, Ser. B, 44*, 533-544, 1992.

Ferm, M., A Na_2CO_3-coated denuder end filter for determination of gaseous HNO_3 and NO_3^- particulate in the atmosphere, *Atmos. Environ.*, *20*, 1193-1201, 1986.

Fuchs, N.A., *The Mechanics of Aerosol*, Pergamon, Tarrytown, N. Y., 1964.

Gerber, H., Direct measurement of suspended particulate volume concentration and far-infrared extinction coefficient with a laser-diffraction instrument, *Appl. Opt.*, *30*, 4824-4831, 1991.

Haynes, D.R., N.J. Tro, and S.M. George, Condensation and evaporation of H_2O on ice surfaces, *J. Phys. Chem.*, *96*, 8502-8509, 1992.

Houdier, S., S. Perrier, E. Defrancq, and M. Legrand, A new fluorescent probe for sensitive detection of carbonyl compounds: Sensitivity improvement and application to environmental water samples, *An. Chem. Acta*, in press, 2000.

Iribarne, J.V., and T. Pyshnov, The effect of freezing on the composition of supercooled droplets, 1, Retention of HCl, HNO_3, NH_3, and H_2O_2, *Atmos. Environ., Part A*, *24*, 383-387, 1990.

Iribarne, J.V., T. Pyshnov, and B. Naik, The effect of freezing on the composition of supercooled droplets, II, Retention of S(IV), *Atmos. Environ., Part A*, 24, 389-398, 1990.

Jacob, D., The chemistry of OH in remote clouds and its role in the production of formic acid and peroxymonosulfate, *J. Geophys. Res.*, *91*, 9807-9826, 1986.

Jaffrezo, J.L., N. Calas, and M. Bouchet, Carboxylic acid measurements with ionic chromatography, *Atmos. Environ.*, *32*, 2705-2708, 1998.

Jayne, J.T., S.X. Duan, P. Davidovits, D.R. Worsnop, M.S. Zahniser, and C.E. Kolb, Uptake of gas-phase alcohol and organic acid molecules by water surfaces, *J. Phys. Chem.*, *95*, 6329-6336, 1991.

Johnson, B.J., E.A. Betterton, and D. Craig, Henry's law coefficients of formic and acetic acids, *J. Atmos. Chem.*, *24*, 113-119, 1996.

Keene, W.C., B.W. Mosher, D.J. Jacob, J.W. Munger, R.W. Talbot, R.S. Artz, J.R. Maben, B.C. Daube, and J.N. Galloway, Carboxylic acids in clouds at a high-elevation forested site in central Virginia, *J. Geophys. Res.*, *100*, 9345-9357, 1995.

Klemm, O., and R.W. Talbot, A sensitive method for measuring atmospheric concentrations of sulfur dioxide, *J. Atmos. Chem.*, *13*, 325-342, 1991.

Knollenberg, R.G., The optical array: An alternative to scattering or extinction for airborne particle size determination, *J. Appl. Meteorol.*, *9*, 86-103, 1970.

Kruisz, C., A. Berner, and B. Brantner, A cloud water sampler for high wind speeds, in *The Proceedings of EUROTRAC Symposium 1992*, edited by P.M. Borrell et al., pp. 523-525, SPB Acad. Publ., The Hague, Netherlands, 1993.

Laj, P., et al., Cloud processing of soluble gases, *Atmos. Environ.*, *31*, 2589-2598, 1997.

Lamb, D., and R. Blumenstein, Measurement of the entrapment of sulfur dioxide by rime ice, *Atmos. Environ.*, *21*, 1765-1772, 1987.

Legrand, M., A. Léopold, and F. Dominé, Acidic gases (HCl, HF, HNO_3, HCOOH, and CH_3COOH): A review of ice core data and some preliminary discussions on their air-snow relationship, in *Chemical Exchange Between the Atmosphere and Polar Snow*, edited by E. Wolff and R.C. Bales, *NATO ASI Ser., Ser. I, 43*, 19-43, 1996.

Lehman, P., I. Xueref, and F. Dominé, Preliminary theoretical investigation of solute retention during riming. In *Proceedings of EUROTRAC Symposium '98*, edited by P.M. Borrell et al., 560-564, WIT Press, Southampton, England, 1999.

Locatelli, J.D., and P.V. Hobbs, Fall speeds and masses of solid precipitation particles, *J. Geophys. Res.*, *79*, 2185-2197, 1974.

Ludlam, F.H., The heat economy of a rimed cylinder, *Q. J. R. Meteorol. Soc.*, *77*, 663-666, 1951.

Munger, J.W., D.J. Jacob, B.C. Daube, L.W. Horowitz, W.C. Keene, and B.G. Heikes, Formaldehyde, glyoxal, and methylglyoxal in air and cloudwater at a rural mountain site in central Virginia, *J. Geophys. Res.*, *100*, 9325-9333, 1995.

Norton, R.B., Measurements of gas phase formic and acetic acids at the Mauna Loa Observatory, Hawaii, during the Mauna Loa Observatory Photochemical Experiment 1988, *J. Geophys. Res.*, *97*, 10,389-10,393, 1992.

Olson, T.M., and M.R. Hoffmann, Hydroxyalkylsulfonate formation: Its role as a S (IV) reservoir in atmospheric water droplets, *Atmos. Environ.*, *23*, 985-997, 1989.

Pandis, S.N., and J.H. Seinfeld, Sensitivity analysis of a chemical mechanism for aqueous-phase atmospheric chemistry, *J. Geophys. Res.*, *94*, 1105-1126, 1989.

Pandis, S.N., and J.H. Seinfeld, Should bulk cloud-water samples obey Henry's law ?, *J. Geophys. Res.*, *96*, 10,791-10,798, 1991.

Ponche, J.L., C. George, and P. Mirabel, Mass transfer at the air/water interface: Mass accommodation coefficients of SO_2, HNO_3, NO_2 and NH_3, *J. Atmos. Chem.*, *16*, 1-21, 1993.

Pruppacher, H.R., and J.D. Klett, *Microphysics of Clouds and Precipitation*, 2nd ed., D. Reidel, Norwell, Mass., 1997.

Reischl, G.P., Measurement of ambient aerosols by the differential mobility analyzer method: Concepts and realization criteria for the size range between 2 and 500 nm, *Aerosol Sci. Technol.*, *14*, 5-24, 1991.

Ricci, L., S. Fuzzi, P. Laj, A. Lazzari, G. Orsi, A. Berner, A. Gunther, W. Jaeschke, M. Wendisch, and B. Arends, Gas-liquid equilibria in polluted fog, *Contrib. Atmos. Phys.*, *71*, 159-170, 1998.

Rosenberg, C., W. Winiwarter, M. Gregori, G. Pech, V. Casensky, and H. Puxbaum, Determination of inorganic and organic volatile acids, NH_3, particulate SO_4^{2-}, NO_3^- and Cl^- in ambient air with an annular diffusion denuder system, *Fresenius Z. Anal. Chem.*, *331*, 1-7, 1988.

Sanhueza, E., M.S. Santana, and M. Hermoso, Gas- and aqueous-phase formic and acetic acids at a tropical cloud forest site, *Atmos. Environ., Part A*, *26*, 1421-1426, 1992.

Snider, J.R., and J. Huang, Factors influencing the retention of hydrogen peroxide and molecular oxygen in rime ice, *J. Geophys. Res.*, *103*, 1405-1415, 1998.

Snider, J.R., D.C. Montague, and G. Vali, Hydrogen peroxide retention in rime ice, *J. Geophys. Res.*, *97*, 7569-7578, 1992.

Song, N., and D. Lamb, Aerosol scavenging by ice in supercooled clouds, in *Precipitation Scavenging and Atmosphere-Surface Exchange*, edited by S.E. Schwartz and W.G.N. Slinn, pp. 63-74, Hemisphere Publ. Co., Washington, D.C., 1991.

Talbot, R.W., A.S. Vijgen, and R.C. Harriss, Measuring tropospheric HNO_3: Problems and prospects for nylon filter and mist chamber techniques, *J. Geophys. Res.*, *95*, 7553-7561, 1990.

Thibert, E., Thermodynamique et cinétique des solutions solides Hcl-H_2O et HNO_3-H_2O: Implications atmosphériques, thèse de doctorat, Univ. Joseph Fourier - Grenoble I, Grenoble, France, 1996.

Thibert, E., and F. Dominé, Thermodynamics and kinetics of the solid solution of HCl in ice, *J. Phys. Chem. B*, *101*, 3554-3565, 1997.

Winiwarter, W., H. Puxbaum, S. Fuzzi, M.C. Facchini, G. Orsi, N. Beltz, K. Enderle, and W. Jaeschke, Organic acid and liquid-phase measurements on Po Valley fall-winter conditions in the presence of fog, *Tellus, Ser. B*, *40*, 348-357, 1988.

Winiwarter, W., B. Brantner, and H. Puxbaum, Comment on "Should bulk cloudwater or fog samples obey Henry's law ?" by S.N. Pandis and J.H. Seinfeld, *J. Geophys. Res.*, *97*, 6075-6078, 1992.

Winiwarter, W., et al., Henry's law and the behavior of weak acids and bases in fog and cloud, *J. Atmos. Chem.*, *19*, 173-188, 1994.

N. Chaumerliac, Laboratoire de Météorologie Physique, OPGC, Université Blaise Pascal, 24 Avenue des Landais, 63177 Aubière Cedex, France.

M. Legrand and D. Voisin, Laboratoire de Glaciologie et Géophysique de l'Environnement, CNRS, 38402 Saint Martin d'Hères Cedex, France. (e-mail:mimi@glaciog.ujf-grenoble.fr)

(Received April 26, 1999; revised August 13, 1999;
accepted September 17, 1999.)